COVER SHEET

Paulmier, Thierry and Bell, John M. and Fredericks, Peter M. (2007) Development of a novel cathodic plasma/electrolytic deposition technique part 2: Physico-chemical analysis of the plasma discharge. *Surface and Coatings Technology* 201(21):pp. 8771-8781.

Development of a novel cathodic plasma/electrolytic deposition technique part 2: Physico-chemical analysis of the plasma discharge

T. Paulmier [a], J.M. Bell [a], P.M. Fredericks [b]*

[a] Centre for Built Environment and Engineering Research, Queensland University of Technology, GPO Box 2434, Brisbane, QLD 4001, Australia

[b] School of Physical and Chemical Science, Queensland University of Technology, GPO Box 2434, Brisbane, QLD 4001, Australia

* *Corresponding author. Tel.* : 0061 7 3864 4298*; Fax.* : 0061 7 3864 2794

E-mail address: j.bell@qut.edu.au

Abstract

A novel plasma system has been developed recently for the deposition of carbon and titanium thin films on metal and metal alloy substrates. Unlike other deposition techniques, the process occurs in liquid precursors and a plasma discharge is created and confined around the cathode in a superheated vapour sheath surrounded by the liquid phase. This paper presents a detailed analysis on the physico-chemical mechanisms underlying this process. A correlation has then been carried out between the voltage / current characteristics of the process and the consecutive physical phenomena occurring during the process (vapour phase formation, plasma discharge initiation and evolution). A description of the different coatings (graphite and titanium dioxide) deposited with this technique has been carried out with an attempt to correlate the structure and composition of these films with the composition and physical characteristics of the plasma discharge. This analysis allowed the

construction of a first dissociation and deposition mechanism for this new plasma system.

Keywords: plasma electrolysis, glow discharge, micro-arc discharge, thin film deposition

1 Introduction

Thin film deposition as a modern material fabrication technique is one of the key technologies in various industrial sectors such as micro-electronics, optical coatings, magnetic and optical data storage devices, anti-static coating, hard-surface coating and more recently solar cells and photo-catalytic sensors [1-5]. A wide range of surface engineering techniques have therefore been developed over the past decades to achieve the demanding technological specifications required in the engineering sector. Current advanced surface engineering methods can be separated into two main categories according to the phase used during the process: the liquid or semi-liquid phase methods and the gaseous or vapour phase methods [6]. The generation of plasma, much used in both methods (in the arc or glow discharge stages) is usually carried out under high vacuum which increases significantly the manufacturing costs. However, the glow discharge method possesses the advantage of working at low temperature, contrary to CVD, and thus achieving more flexibility for the structure and morphology of the produced film.

A new plasma electrolytic deposition technique has been developed during the past few years in anodic [7-10] and cathodic [11-16] configuration. This technology is based on contact glow discharge electrolysis phenomena, thoroughly developed and studied by several authors over the past 40 years [17-21]. Operating at atmospheric pressure, the film deposition is activated on the smaller electrode by the formation of

a plasma glow discharge within a gaseous sheath produced in an electrolytic bath around this electrode. Hence, this process combines different deposition mechanisms, which may include mechanisms found in CVD, PECVD, electrophoresis, cataphoresis, ion implantation and sputtering. Used in anodic configuration, this plasma electrolytic technique, also called ‘micro-plasma oxidation’ or ‘anode spark electrolysis’, allows the production of thin adherent oxide, nitride or carbide films [7-9].

In cathodic configuration, this plasma process allowed the production of carbon, titanium, molybdenum, zinc and zinc-aluminium based coatings on metal substrate [11-16]. Nano-crystalline graphite films have been deposited by the authors on a Ti, Al or Cu cathodic substrate from solutions composed of ethanol, potassium chloride and phosphate buffer [22]. The high field emission observed with these graphite films could have application for the manufacturing of high field emission electrodes for plasma devices such as microwave reactors. Highly crystalline titanium dioxide films, composed mainly of anatase and rutile, have been also produced with this technique using a solution composed of titanium tetra-isopropoxide (TTIP) and ethanol [12, 13]. The nano-structure of these films, composed of nano-rods and nano-fibrils, and their composition are very promising for applications in photocatalysis and dye-sensitised solar cells. An interesting feature for these films is that it is possible to adjust their crystallinity and morphology by adjusting the working voltage, and hence the intensity of the plasma discharge.

The production and technology of such a plasma discharge in a vapour phase surrounded by a liquid electrolytic phase is very new and the observation and understanding of this process has been necessary to enhance the potential development of this technique for the production of new advanced materials. This

paper presents therefore a thorough investigation of the physico-chemical implied mechanisms in parallel with the voltage / current characteristics of this process. The formation and evolution of the vapour sheath and the plasma discharge have been analysed using a high speed camera. The plasma composition and electron temperature have moreover been evaluated by emission spectroscopy and correlated with the structure observed in the titanium dioxide films, allowing the construction of a first dissociation and deposition model.

2 Experimental set-up

The basic principle of the cathodic plasma electrolytic process is to apply a high DC voltage between two electrodes immersed in an electrolyte solution. This process operates at atmospheric pressure. In the configuration studied in this work, the cathode surface area being much smaller than the anode surface area ($A_{cathode}/A_{anode} \approx 0.08$), the electric field is higher near the cathode inducing a strong Joule heating in the vicinity of this electrode, the formation of a vapour shield around it and the initiation of a plasma discharge within the vapour phase.

The plasma electrolytic reactor is composed of a jacketed glass vessel with an inner volume of 1 litre (figure 1). This vessel is cooled by a water flow in order to control and adjust the temperature of the liquid solution. A set of electrodes is maintained within the liquid solution by two copper and stainless steel supports which also allow connection to the electrical power supply. The length of the centred cathode is adjusted at 10 mm using a 100 mm long Teflon shield. The cathode is a 3.1 mm diameter copper rod. The surrounding anode is a 40 mm inner diameter cylinder composed of graphite to avoid any oxidation of the anode and any metallic deposition of anodic element on the cathode. This plasma reactor works at

atmospheric pressure and is blanketed by a continuous flow of nitrogen to avoid any flames or explosion within the glass vessel. The reactor is powered by a DC power supply (Bertran 105-02R) with a maximum voltage of 2000 V, a maximum power output of 1kW and a maximum current of 500 mA. The applied voltage needed to achieve the vapour sheath around the cathode and initiate a stable glow discharge all along the cathode mainly depends on the composition of the solution and its conductivity. In the work presented here, this voltage is in the range 400 to 1200 V. The current density at the cathode is normally around 0.25-0.5 A cm^{-2}. The temperature of the solution within the reactor is measured during the process using a conventional mercury thermometer. To keep the same volume of solution during the tests, a condenser, cooled by water flow, has been installed at the top of the reactor. An external solution tank, pressurised with nitrogen, has also been installed and connected to the plasma reactor by a 3 mm inner diameter Teflon tube in order to add a given quantity of solution during the process. For the voltage / current analysis and the study on the basic physical mechanisms (vapour sheath and plasma discharge), the solution was composed of absolute ethanol (96 % vol.), phosphate buffer (4 % vol.) and potassium chloride (0.2 mol/l). The reason is that this solution remains clear for a sufficiently long time to analyse the physical phenomena occurring during the different voltage / current stages.

The formation of the vapour sheath, the physical characteristics of the plasma discharge and their evolution with the applied voltage have been studied using a high speed camera (Photron 512 PCI FastCam-X) shot at 2000 frames per second (shutter: 1/2500 sec).

In-situ optical emission spectroscopy (OES) was carried out on the plasma discharge using a S2000-UV-VIS Miniature Fibre Optic Spectrometer (Ocean Optics

Inc.) with 200-850 nm wavelength range. The spectrometer was connected to a PC through a RS232 connection for the control of the spectrometer and the data acquisition. The acquisition time used during the measurements was 10 s. A special reactor was set-up in order to get the fibre optics as close as possible to the plasma discharge without immersing the fibre in the liquid solution. A glass hollow finger, where the fibre optics was introduced, was inserted into a glass reaction flask to place the fibre at around 5 mm from the axis centre, where the cathode was located (figure 2). For the emission spectroscopy study, we used a solution composed of 100 cm^3 of distilled titanium tetraisopropoxide (TTIP, $Ti(OC_3H_7)_4$, Sigma-Aldrich, 97 %), 150 cm^3 of absolute ethanol and 0.6 cm^3 of hydrochloric acid (HCl) (concentration: 31.5 % w/w). The cathode was treated in the plasma reactor for 300 seconds at a maximum voltage varying from 600 to 1000 V. The produced titania coatings have then been analysed after treatment.

The morphology of the produced coatings has been studied by SEM using a FEI Quanta 200 Environmental SEM. Surface analysis was carried out on the films without further preparation. The composition and crystallinity of the films were studied by Raman spectroscopy. Visible Raman spectra were measured using a Renishaw InVia Raman microprobe spectrometer equipped with laser excitation at 532 nm (20 mW at the sample) and a 50x microscope objective.

3 Results and discussion

3.1 Overview and presentation of the deposited materials

The process has been used by the authors to produce graphite like carbon and nano-structured titanium dioxide coatings. The graphite films have been produced using a solution composed of absolute ethanol, phosphate buffer and potassium chloride.

These carbon coatings present a rough surface looking like the result of the fusion of micro-particle clusters. This surface is then composed of a large quantity of crevices and micro-buckles. Figure 3 presents the SEM picture of the carbon coating produced at 1000 V. The titanium dioxide coatings have been deposited by treating a liquid solution composed of 100 cm^3 of distilled titanium tetraisopropoxide, absolute ethanol and hydrochloric acid. The cathode was treated in the plasma reactor at three different voltages (600, 700 and 1000 V). From figure 4, we can notice that the morphology of the coatings strongly varies with the applied voltage. At 600 V (figure 4a), the coating is composed of TiO_2 nano-fibres, with an average diameter equal to 200 nm. These fibres tend to acquire the same orientation, perpendicular to the substrate surface. At 700 V, the nano-fibers have fused together forming a dense and granular coating (figure 4b). We can still observe the presence of protruding nano-fibres at the surface of the coating. At 1000 V, the produced TiO_2 coatings are very dense and thick: they present a network of entangled grooves and crevices. The observation of this coating by Trasmission Electron Microscopy reveals that this coating is the results of build-up and fusion of numerous titania nano-particles. The average size of these nano-particles is around 25 nm.

The analysis of the coatings by visible Raman spectroscopy reveals that their crystallinity increases significantly with the applied voltage (figure 5). At 600 V, the film is then composed of anatase (observed from the E_g vibration peak at 152 cm^{-1}) and amorphous titanium dioxide characterised by the four very broad peaks at 190, 426, 598 and 890 cm^{-1}. Two other peaks at 1330 and 1588 cm^{-1} coming from graphite-like carbon appear as well in this coating. This graphite can come from the dissociation of ethanol or the isopropyl group present in TTIP. For voltages above 600 V, the deposited coatings are highly crystallised composed of a mixture of

anatase (peaks at 152, 199, 390, 504 and 626 cm^{-1}), rutile (peaks at 442, 607 and 803 cm^{-1}) [23-25] and graphite-like carbon.

3.2 The bubble sheath formation

Figure 6 shows the evolution of the voltage and current, as well as representations of the different physical phenomena occurring at each step of the process. In a first stage (A-B in Figure 6), the solution is heated by the Joule effect. Figure 7 shows the evolution of the liquid temperature in the vicinity of the anode (20 mm from the cathode). We observe that the bulk temperature of the solution increases with the current, up to the vaporisation temperature of the solution at 351 K. The overall solution is thus rapidly heated with the increasing current.

In a first approximation, the electric field between the two electrodes can be written in a cylindrical coordinate system:

$$\vec{E} = \frac{V_2 - V_1}{\ln\left(\frac{r_2}{r_1}\right)} \frac{1}{r} \vec{u}_r \quad \textbf{(1)}$$

The Joule heating flux, given by $\Phi = \sigma.E^2$, is then concentrated around the cathode. During this stage, the solution is subject to strong and rapid heating, which is especially intense at the surface of the cathode. Some small bubbles are especially emitted at the tip of the cathode where the electric field is the highest.

From figure 6 it can be seen that the current actually shows a super-linear evolution. This characteristic is due to the increase of the electric conductivity of the solution with temperature. Assuming that the temperature increase is uniform throughout the entire solution volume, we can estimate the evolution of the current in

this region by calculating the temperature increase ΔT(t) in the interval t to t+Δt from the power input ΔQ(t) in this time and the heat capacity of the solution C:

$$\Delta T\ (t) = \frac{\Delta Q(t)}{v.\rho.C} \quad where\ \Delta Q(t) = \int_{t}^{t+\Delta t} V(t')I(t')dt'$$

, ν is the solution volume between the two electrodes and ρ the density of the solution

Further assuming a linear relationship between conductivity and temperature ($\sigma(T+\Delta T) = \sigma(T) + \alpha_T.\Delta T$), with α_T a constant over the temperature range involved (270-350K), we can determine the evolution of the current. We have performed this calculation from the data in figure 6, and obtained the resultant I-t curve shown in figure 8, for an initial conductivity σ_0 = 265μS/cm and α_T=18μS/cm. This simplified model, which does not take into account the spatial variation in temperature in the electrolyte and heat transfer processes, nevertheless clearly demonstrates the dominant contribution to the origin of the superlinear current evolution.

When the bulk temperature reaches the vaporisation one, the saturation temperature necessary to initiate the nucleation and formation of bubbles is reached at the vicinity of the cathode. The nucleation of bubbles all along the surface starts actually at point B (figure 6). It is initiated at this point, starting at the tip and moving to the end of the cathode. The transition from point B to point C corresponds to the displacement of the bubble front from the tip to the end of the cathode. At point C, the cathode is then completely covered by a vapour sheath, composed of a cluster of bubbles, which eventually isolates totally the electrode from the liquid electrolyte. This vapour sheath is formed very quickly, in a few milliseconds. It is not continuous and can be considered as a composite of gas and liquid phases (figure 9). The effective conductivity σ_{eff} of the gas-liquid composite can be approximated by the

Bruggeman relation, which is usually referred to in the electrochemical literature [26, 27]:

$$\sigma_{eff} = \sigma_L.(1-\alpha)^{3/2} \qquad (2)$$

where σ_L is the electrical conductivity of the liquid solution without bubbles and α the volume fraction of bubbles.

Once the vapour sheath is formed, the electric conductivity of this overheated layer increases leading to an increase of the total electric resistance of the liquid – vapour system and thus to a quasi instantaneous current fall (region BC). We can notice in figure 9 that the gas phase fraction of the bubble sheath as well as the vapour thickness rise with the increasing applied voltage (region CD). In other terms, as the voltage increases, the electric resistance of the composite vapour phase significantly soars up: the main voltage drop occurs rapidly within the vapour sheath resulting in a decrease of the current intensity.

The increase of the vapour thickness is due to two physical phenomena: coalescence and electrostatic pressure effect. We have indeed observed the coalescence of the bubbles at the cathode surface forming a discrete, then a long vapour column (or vapour mushrooms) along or perpendicular to the surface (see figure 9, especially at 600 V). Two kinds of coalescence processes have to be distinguished: lateral coalescence and longitudinal coalescence [28, 29]. Lateral coalescence corresponds to the coalescence of bubbles growing on the surface at neighbouring nucleation sites. Coalescence in the direction normal to the surface of bubbles originating from the same nucleation site is called longitudinal coalescence. In this case, the growth speed of the second bubble is higher than the bulk speed of the first bubble, which leads to the impact between the two bubbles and to their

coalescence. These two types of bubbles coalescence have both been observed during the transition stage (region CD).

Furthermore, once initiated, the bubbles are subject to different internal and external pressures due to the electric field, exerted respectively in the gas and the liquid phase. As the effective resistance of the vapour sheath increases, the inner electric field will be enhanced inducing an overpressure within the bubble which will stimulate its growth.

We have met some difficulties in distinguishing coalescence and electrostatic pressure effect on the enlargement of the vapour sheath. The main reason is that the electric field is both responsible for the vaporisation of the liquid solution, bringing about strong coalescence, and for the internal electrostatic pressure which expands the bubble.

At point D, the voltage drop within the vapour sheath is sufficiently high to promote the ionisation of the gas and initiate consecutive plasma discharges within the different bubbles. The behaviour of the electric current is then steered by the physical characteristics of the plasma discharge which are discussed in the following part.

3.3 The plasma discharge characteristics

At point D in figure 6, the main voltage drop has been evaluated numerically equal to 694 V for a total applied voltage of 790 V. Hence, at the end of the transition stage, the main voltage drop occurs primarily within the vapour sheath. As the liquid phase conductivity is much higher than the vapour sheath conductivity, the vapour phase-liquid interface acts as the anode: the effective distance between the anode and the cathode is then equal to 0.1- 5 mm (bubble diameter) at point D. The breakdown voltage V_b of a gas, which is critical in the initiation of a discharge, strongly depends on the product of pressure and distance p.d [30]:

$$V_b = \frac{B(p.d)}{Ln[A(p.d)] - Ln[Ln(1+1/\gamma_{se})]} \quad \textbf{(3)}$$

A and B are constants found experimentally and γ_{se} is the secondary electron emission coefficient of the cathode. For values of p.d higher than 10 (in Torr.cm), the breakdown voltage increases rapidly with the inter-electrode gap at constant pressure. V_b is usually lower than 1000 V for p.d lower than 10 [30]. We have been able to show, by high speed camera measurements, that the plasma discharges are actually initiated in very small bubbles presenting a diameter equal to around 0.1 mm. In our experiment, the tests are carried out at atmospheric pressure (760 Torr) and at voltages lower than 1200 V. In a very small diameter bubble (around 0.1 mm), the effective p.d product will be sufficiently low (equal to 7.6 Torr.cm for a bubble diameter of 0.1 mm) to ensure a low breakdown voltage and initiate the formation of a plasma discharge within the small bubble.

If we increase the voltage again beyond the breakdown point, we observe an increase of the current (region DE), explained by the increasing cathode surface area treated by the plasma discharge, as we can see in figure 10. At point E, the plasma discharge occurs across the entire cathode surface.

For a voltage equal to or above 900 V, the cathode surface is entirely covered by the plasma glow discharge, as seen in figure 10b. This figure shows that the plasma system is actually composed of a superposition of several small discharges along the substrate. Moreover, even submitted to a contraction by the bubble, the plasma discharge remains in a diffuse form, characteristics of a ‘glow’ discharge [31].

The conductivity of the plasma discharge is much higher than the conductivity of the surrounding vapour phase, owing to the ionisation of the vapour. Therefore the

current measured between the two electrodes corresponds to the total current in all the multiple micro-plasma discharges. The vapour layer surrounding the plasma discharge acts like an insulating component and does not contribute to the electric current. Figure 11 shows the evolution of the current with the applied voltage for the same electrolyte, but with the voltage held constant beyond point E (see Figure 6) at three different voltages – 900V, 1000V and 1200V. The current increases with the applied voltage once the plasma discharge is established across the cathode. The mean current at 900, 1000 and 1200 V is equal to 268, 300 and 350 mA respectively for a total surface area equal to 1.07 cm^2. It is then possible to calculate voltage and power in the plasma discharge for each applied voltage (table 1). Once the surface is totally covered by the plasma discharge, increasing the voltage implies extracting more electrons per unit surface area, leading to an increase of the current density and the discharge power density. At the same time, the luminous intensity of the plasma discharge increases significantly. The current/voltage characteristics, the range of the current (hundreds of mA per cm^2) and discharge power, and the physical shape of the discharge are all akin to the features of an abnormal glow discharge [30, 31].

The temporal evolution of the plasma discharge has been studied using a sharp tip cathode in order to obtain the best picture quality and to observe accurately the evolution of the plasma discharge. Figure 12 illustrates the temporal evolution of the plasma discharge: the plasma discharge is initiated within bubbles with very small diameter (around 0.1 mm). The high electric field within this very small bubble is sufficiently high (around 100 $kV.cm^{-1}$) to induce the breakdown of the gas leading to a plasma discharge. We propose that the relatively high temperature of the initial discharge induces a dramatic increase of the vaporisation rate of the electrolyte liquid solution around the bubble. Due to this high vaporisation rate, the bubble diameter

and the plasma discharge enlarge rapidly, in a few milliseconds, as we can see in figure 12. The expansion of the bubble is caused as well by the plasma pressure exerted at the surface of the bubble. This plasma pressure is expressed by the relation:

$$P_p = \sum_k n_k k T_k = n_e k T_e + n_p k T_p + n_0 k T_0 \qquad \textbf{(4)}$$

with n_e: electron density, n_p: ion density, n_0: neutral particle density, T_e: electron temperature, T_p: ion temperature, T_0: neutral temperature.

The total force is the sum of the plasma pressure acting inside the bubble and the electrostatic pressure acting outside the bubble (in the liquid phase). As the voltage drop mainly occurs within the vapour sheath, the electric field within the liquid solution is very low: we therefore believe that the electrostatic pressure in the liquid phase is negligible compared to the inner plasma pressure. The total electrostatic pressure thus tends to expand the bubble and the plasma discharge.

Once the bubble volume is sufficiently large, the buoyancy force will overcome the plasma pressure within the bubble. The bubble then moves upward until the discharge subsides, as observed in figure 12 (time 27.5 ms). Another discharge is then initiated in a very small diameter bubble. We can then observe the succession of several abnormal glow discharges formed within the gas phase. This rapid succession of discharge events is responsible for the large fluctuation of the current intensity observed in the current/voltage characteristics.

Using a TTIP liquid solution, the electron temperature has been calculated at 700 and 1000 V from the emission spectra measured on the plasma discharges (figure 13). The plasma discharge is mainly composed of Ti radicals, coming from the dissociation of the TTIP solution, oxygen species, hydrogen and water molecules. Three titanium lines, whose parameters are listed in table 2, have been used to

calculate the electron temperature using the Boltzmann plot method [32]. This method requires a pair of line emitted by the same species. If we assume that the plasma discharge is in local thermal equilibrium (LTE), which is generally the case for a plasma discharge produced at atmospheric pressure, the electron temperature T_e is given by the relation:

$$T_e = \frac{E_2 - E_1}{k_B}\left[Ln\left(\frac{I_1.\lambda_1.g_2.A_2}{I_2.\lambda_2.g_1.A_1} \right) \right]^{-1} \quad \textbf{(5)}$$

where k_B is the Boltzmann constant, I_i the measured intensity of line i, λ_i its wavelength, E_i the energy of the excited state, g_i its statistical weight and A_i the transition probability.

We have used the intensity ratio measurements between line 1 and 3 and between line 2 and 3 (see table 2). The spectral transmission of the glass and liquid solution is approximately continuous in the spectral range covered by these three titanium lines. The electron temperature is relatively the same for the two studied voltages, equal to 1 eV. This temperature level is a physical characteristic of a plasma glow discharge and is relatively low compared to hot plasma and arc discharges where the electron temperature can reach 2 to 3 eV. The main difference between the two applied voltages may lie in the electron density which should increase with the voltage. Due to the confinement of the plasma discharge and the liquid medium surrounding the discharge, the evaluation of this density remains however a very tedious operation.

3.4 The dissociation mechanisms

From the previous experimental analysis on the plasma discharge and the analysis on the produced TiO_2 coatings, we have tried to deduce the dissociation and deposition mechanisms leading to the formation of this coating. In a first step, we can assert that

the plasma discharge is directly responsible of the formation of the titanium dioxide coating since no deposit have been observed without the presence of the plasma discharge. The TTIP solution needs therefore to be heated, vaporised around the cathode and treated by the plasma discharge. It is therefore wise to say that the deposition mechanisms are mainly ruled by the plasma processes.

We have found out from the emission spectroscopy of the plasma that TTIP is entirely decomposed in the plasma discharge into titanium radicals. The TTIP can be dissociated within the plasma discharge by four different processes: the photo-dissociation, the electron impact dissociation, the ion impact dissociation and the thermal impact dissociation [33]. We can assume that the thermal dissociative processes play a significant role in the deposition mechanism: we have indeed demonstrated previously that the plasma discharge produced in our experimental conditions is an abnormal glow discharge. This basically means that the temperature of neutral and ionised species is relatively high (500 K or higher) due to the high energy exchange by collision between the electrons and the molecule and ions of the gas [30]. The degree of ionisation caused by the generated electrons remains however relatively low making the electron impact dissociation process negligible in regard of the thermal one. Submitted to the high plasma temperatures, the surface of the cathode is strongly heated and vaporised TTIP is then thermally dissociated at the surface of the cathode. Cho et al. [34] have studied the thermal decomposition mechanisms of TTIP. They have demonstrated that TTIP can be adsorbed at the surface of a heated substrate and then dissociated according to the scheme:

$$\begin{cases} Ti(OC_3H_7)_4 \rightarrow Ti(OC_3H_7)_4* \\ Ti(OC_3H_7)_4* \rightarrow Ti(OC_3H_7)_{4-x}* + x(OC_3H_7)* \\ \ldots \\ Ti-OC_3H_7* \rightarrow Ti-OH + C_3H_6 \\ 2Ti-OC_3H_7* \rightarrow 2Ti* + HOC_3H_7 + OC_3H_6 \\ 2Ti-OC_3H_7* \rightarrow Ti* + OC_3H_6 + 1/2H_2 \\ \\ OC_3H_7* \rightarrow C_3H_6O + H* \\ R-CH_3* \rightarrow R* + C* + 3H* \end{cases} \quad \textbf{(6)}$$

This model is in good agreement with the observation carried out on the plasma discharge by emission spectroscopy. In accordance with this model, we have indeed observed a high concentration of Ti radicals and the presence of hydrogen (H alpha line). Furthermore, the analysis of the produced coatings have revealed the presence of graphite-like coming, according to this model, from the thermal dissociation of the volatile hydrocarbons, products of the TTIP decomposition.

It has also been demonstrated [35, 36] that TTIP can be thermally decomposed in the gas phase to form particles of TiO_2 according to the following reactions:

$$\begin{aligned} &Ti(OC_3H_7)_4 \rightarrow TiO_2 + 2C_3H_6 + 2HOC_3H_7 \quad for\ T < 673\ K \\ &Ti(OC_3H_7)_4 \rightarrow TiO_2 + 4C_3H_6 + 2H_2O \quad for\ T \geq 673\ K \end{aligned} \quad \textbf{(7)}$$

In our case, we have demonstrated that the temperature of the plasma discharge is sufficiently high (around 623 K or higher) to produce a mixture of anatase and rutile at the surface of the cathode. This temperature is therefore sufficiently high to decompose the vaporized TTIP according to reactions (7) and form crystallized nano-particles that are then chemically adsorbed at the surface of the cathode.

For temperature above 623 K, we can see that reaction 7 leads to the formation of water in the gas phase. Several studies on contact glow discharge electrolysis [18, 20, 37] have shown that water molecules can interact with the plasma discharge to produce O_2, H_2 and H_2O_2.

$$\begin{cases} H_2O \xrightarrow{plasma} H^\bullet + OH^\bullet \\ H^\bullet + H^\bullet \rightarrow H_2 \\ OH^\bullet + OH^\bullet \rightarrow H_2O + 1/2O_2 \\ \\ OH^\bullet + OH^\bullet \rightarrow H_2O_2 \\ OH^\bullet + H_2O_2 \rightarrow HO_2^\bullet + H_2O \\ OH^\bullet + HO_2^\bullet \rightarrow H_2O + O_2 \end{cases} \quad \textbf{(8)}$$

The presence of O_2 at the cathode within the plasma discharge has indeed been detected by emission spectroscopy. This oxygen will rapidly react in the vapour sheath with the titanium radicals produced from reactions (5) and adsorbed at the surface to produce TiO_2.

The reaction scheme described here should be completed by the possible photon or ion impact dissociation process. A future comprehensive analysis of the plasma discharge (by ultraviolet spectroscopy), the liquid solution and the gas phase, is however necessary to achieve this task.

4 Summary and conclusion

This paper presents an analysis of the physico-chemical mechanisms underlying a novel plasma electrolytic system which has been developed over the past few years to deposit thin films on a cathodically-biased substrate. As for any film

deposition technique, the control and adjustment of the quality and structure of the produced films requires a good understanding on the plasma phenomena occurring during the deposition.

In this paper, we have been able to demonstrate that the vapour sheath, result of the vaporisation of the adjacent liquid layer around the cathode, is submitted to a strong ionisation process leading to the initiation of a plasma discharge within this gas phase. The physical characteristics of this plasma glow discharge (electron temperature, current density, plasma power, current / voltage characteristics) are the signature of an abnormal glow discharge. Due to the high temperature involved within this type of plasma, the vaporised titanium isopropoxide or ethanol solutions are submitted to a significant plasma chemical dissociation at the surface of the plasma-heated cathode. These processes induce the formation of nano-structured crystalline titanium dioxide or graphite coatings at the surface of the cathode.

The advantage of this plasma electrolytic discharge for film deposition is that we can obtain novel and different structures and crystallinities by adjusting the electric operating parameter of the system. The high deposition kinetic, the operation at atmospheric pressure (without any supply of additional oxygen), the direct production of crystalline coatings without further post-deposition annealing make this technique very efficient, cheap compared to the other more conventional techniques and thus the technique is industrially very attractive.

This study provides a foundation for future optimisation and control of this process. Further studies are necessary to have a comprehensive understanding on the plasma chemical dissociation processes including the photon, electron and ion impact dissociation phenomena. This step implies a complete experimental characterisation of the entire system (analysis and evolution of the liquid, gas and plasma

composition) and the development of a theoretical model describing the overall plasma deposition mechanisms.

Acknowledgment

Support for this project from the Australian Research Council Discovery Grant DP0345956 is gratefully acknowledged.

References

[1] K. Seshan, Handbook of Thin-Film Deposition Processes and Techniques - Principles, Methods, Equipment and Applications (2nd Edition), William Andrew Publishing/Noyes (2002)

[2] R.F. Bunshah, Handbook of Deposition Technologies for Films and Coatings - Science, Technology and Applications (2nd Edition), William Andrew Publishing/Noyes (1994)

[3] A. Goetzberger, C. Hebling, H.-W. Schock, Mater. Sci. Eng., R 40 (2003) 1

[4] D. P. Norton, Mater. Sci. Eng., R 43 (2004) 139

[5] U. Diebold, Surf. Sci. Rep. 48 (2003) 53

[6] D.S Rickerby, A. Matthews, Advanced Surface Coatings: a Handbook of Surface Engineering, Blackie and Son Ltd (1991)

[7] L. O. Snizhko , A. L. Yerokhin , A. Pilkington , N. L. Gurevina , D. O. Misnyankin , A. Leyland, A. Matthews, Electrochim. Acta 49 (2004) 2085

[8] X. Nie, C. Tsotsos, A. Wilson, A. L. Yerokhin, A. Leyland, A. Matthews, Surf. Coat. Technol. 139 (2001) 135

[9] A. L. Yerokhin, X. Nie, A. Leyland, A. Matthews, Surf. Coat. Technol. 130 (2000) 195

[10] A. L. Yerokhin, X. Nie, A. Leyland, A. Matthews, S. J. Dowey, Surf. Coat. Technol. 122 (1999) 73

[11] E. L. Izake, T. Paulmier, J. M. Bell, P. M. Fredericks, J. Mater. Chem. 15 (2005) 300

[12] T. Paulmier, E.L. Izake, C. Runge, J. Bell, P. Fredericks, Mater. Forum 29 (2005) 71

[13] T. Paulmier, C. Runge, E. Kiriakos, P. Fredericks, J.M. Bell, Proceedings of the 19th International Conference on Raman Spectroscopy (ICORS), Surfers Paradise (Australia), PM Fredericks, R Frost and L. Rintoul (Eds.), CSIRO Publishing, (August 2004), pp 564-565

[14] T. Paulmier, E. Kiriakos, J.M. Bell, P. Fredericks, Proceedings of the 28th Annual Condensed Matter and Materials Meeting, Wagga-Wagga (Australia), edited by The Australian Institute of Physics (January 2004) : www.aip.org.au/wagga2004/

[15] E. I. Meletis, X. Nie, F. L. Wang, J. C. Jiang, Surf. Coat. Technol. 150 (2002) 246

[16] P. Gupta, G. Tenhundfeld, E.O. Daigle, P.J. Schilling, Surf. Coat. Technol. 200 (2005) 1587

[17] A. Hickling, M. Ingram, Trans. Faraday Soc 60 (1964) 783

[18] A. Hickling, Modern Aspects of Electrochemistry **6** (1971), eds. J. O'M. Bockris, B. E. Conway, pp 329-373

[19] H. Kellogg, J. Electrochem. Soc. 97 (1950) 133

[20] S.K. Sengupta, R. Singh, A.K. Srivastava, J. Electrochem. Soc. 145 (1998) 2209

[21] S.K. Sengupta, A.K. Srivastava, R. Singh, J. Electroanal. Chem. 427 (1997) 23

[22] T.Paulmier, J.M. Bell, P.M. Fredericks, Deposition of nano-crystalline graphite films by cathodic plasma electrolysis, submitted to Thin Solid Films

[23] V.V. Yakovlev, G. Scarel, C.R. Aita, S. Mochizuki, Appl. Phys. Lett. 76 (2000) 1107

[24] M. Ocaña, J.V. Garcia-Ramos, C.J. Serna, J. Am. Ceram. Soc. 75 (1992) 2010

[25] W.-X. Xu, S. Zhu, X.-C. Fu, Q. Chen, Appl. Surf. Sci. 148 (1999) 253

[26] H. Vogt, H.-D. Kleinschrodt, J. Appl. Electrochem. 33 (2003) 563

[27] A. A. Dahlkild, J. Fluid Mech. 428 (2001) 249

[28] Y. A. Buyevich, B. W. Webbon, Int. J. Heat Mass Transfer 40 (1997) 365

[29] J. Bonjour, M. Clausse, M. Lallemand, Exp. Therm Fluid Sci. 20 (2000) 180

[30] A. Schutze, J.Y. Jeong, S.E. Babayan, P. Jaeyoung, G.S. Selwyn, R.F. Hicks, IEEE Trans. Plasma Sci. 26 (1998) 1685

[31] Y. P. Raizer, Gas discharge Physics, Chapter 8: Stable glow discharge, Springer Verlag (Berlin Heidelberg), 1991, pp 167-213

[32] A. Descoeudres, C. Hollenstein, R. Demellayer, G. Wälder, J. Phys. D : Appl. Phys. 37 (2004) 875

[33] J.-S. Chang, A.J. Kelly, J.M. Crowley, Handbook of Electrostatic Processes, Marcel Dekker Inc., New York (1995)

[34] S.-I. Cho, C.-H. Chung, S.H. Moon, Thin Solid Films 409 (2002) 98

[35] U. Backman, A. Auvinen, J.K. Jokiniemi, Surf. Coat. Technol. 192 (2005) 81

[36] C.P. Fictorie, J.F. Evans, W.L. Gladfelter, J. Vac. Sci. Technol. A 12 (1994) 1108

[37] J. Gao, X. Wang, Z. Hu, H. Deng, J. Hou, X. Lu, J. Kang, Water Res. 37 (2003) 267-272

FIGURE CAPTIONS

Figure 1: Scheme of the plasma reactor. 1: Cathode support, 2: Anode, 3: Jacketed glass vessel, 4: Water inlet, 5: Teflon shield, 6: Solution addition, 7: Thermometer, 8: Solution sampling system, 9: Gas exhaust, 10: Treated Cathode

Figure 2: Experimental set-up used for the emission spectroscopy measurements

Figure 3: SEM picture of the graphite coating produced at 1000 V from a solution composed of absolute ethanol, phosphate buffer and potassium chloride

Figure 4: SEM pictures of the titanium dioxide coatings produced for 300 seconds from a solution composed of TTIP (40%), ethanol (58.8 %) and HCl (0.2 %) and treated at: (a) 600 V, (b) 700 V, (c) 1000 V

Figure 5: Visible Raman spectra of the titanium dioxide coatings produced at 600 V, 700 V and 1000 V from a solution composed of TTIP (40%), ethanol (58.8 %) and HCl (0.2 %)

Figure 6: Evolution of voltage and electric current with time for an ethanol solution treated at 1000 V (voltage ramp rate: 3V/s)

Figure 7: Evolution of the temperature, current intensity and electric power with time during the heating stage for an ethanol solution treated at 1000 V (voltage ramp rate: 3V/s)

Figure 8: Theoretical evolution of the electric current (linear and super-linear) and the electric conductivity of the solution during the joule heating stage of the plasma electrolytic process

Figure 9: Evolution of the vapour sheath with the applied voltage for an ethanol solution

Figure 10: Feature of the plasma discharge imaged using a high speed camera for an ethanol solution treated at: (a) 800 V, (b) 900 V

Figure 11: Temporal evolution of the current intensity according to the applied voltage

Figure 12: Evolution of a plasma discharge within a bubble for an ethanol solution treated at 1300 V

Figure 13: Emission spectrum of the plasma discharge produced in a solution composed of TTIP (40%), ethanol (58.8 %) and HCl (0.2 %) and treated at 700 and 1000 V

CAPTION OF TABLES

Table 1: Evolution with the applied voltage of current, voltage and electric power in the plasma discharge

Table 2: Theoretical titanium line parameters used for the determination of electron temperature

FIGURES

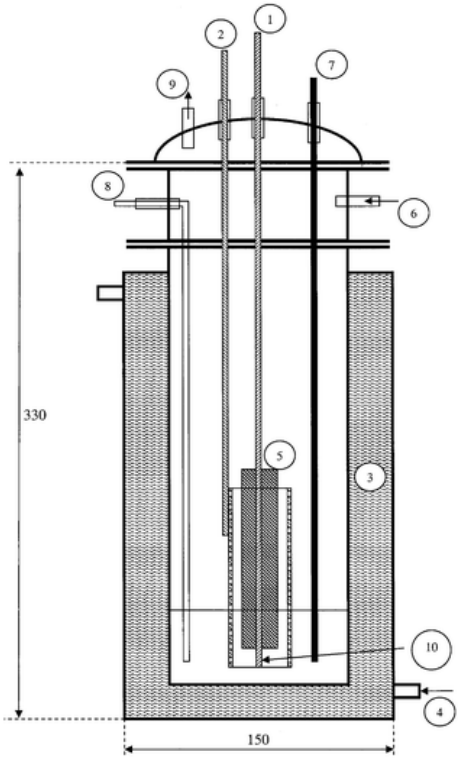

Figure 1

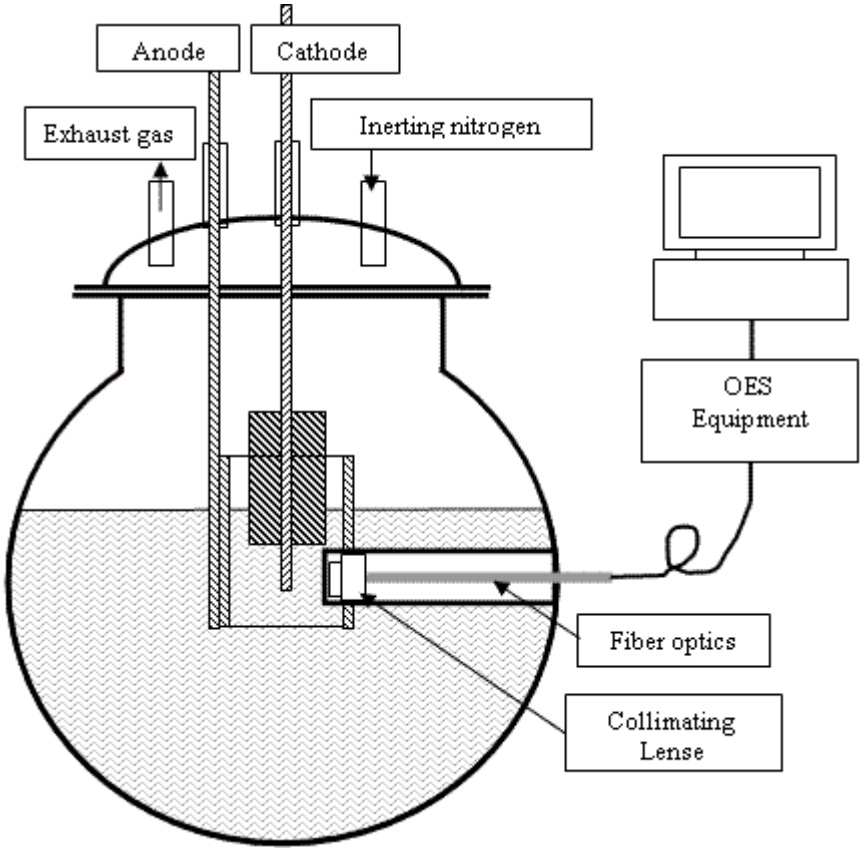
Anode
Cathode
Exhaust gas
Inerting nitrogen
OES
Equipment
Fiber optics
Collimating
Lense

Figure 2

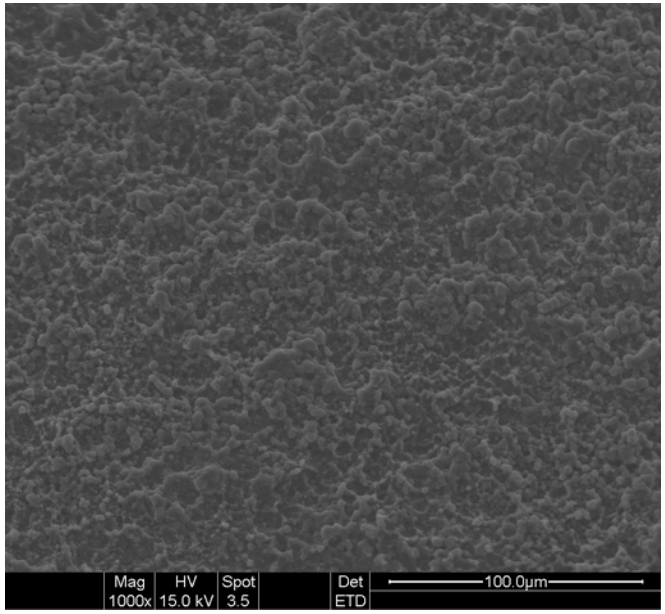

Figure 3

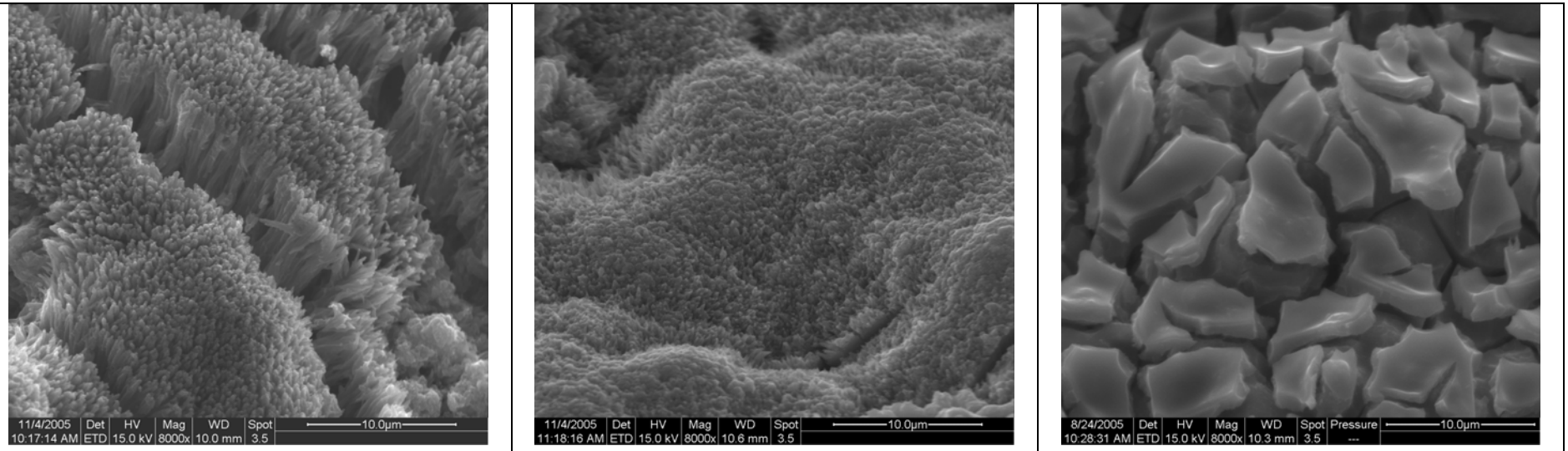
11/4/2005 Det HV Mag WD Spot
10:17:14 AM ETD 15.0 kV 8000x 10.0 mm 3.5
10.0µm
11/4/2005 Det HV Mag WD Spot
11:18:16 AM ETD 15.0 kV 8000x 10.6 mm 3.5
10.0µm
8/24/2005 Det HV Mag WD Spot Pressure
10:28:31 AM ETD 15.0 kV 8000x 10.3 mm 3.5 ---
10.0µm

(a) (b) (c)

Figure 4

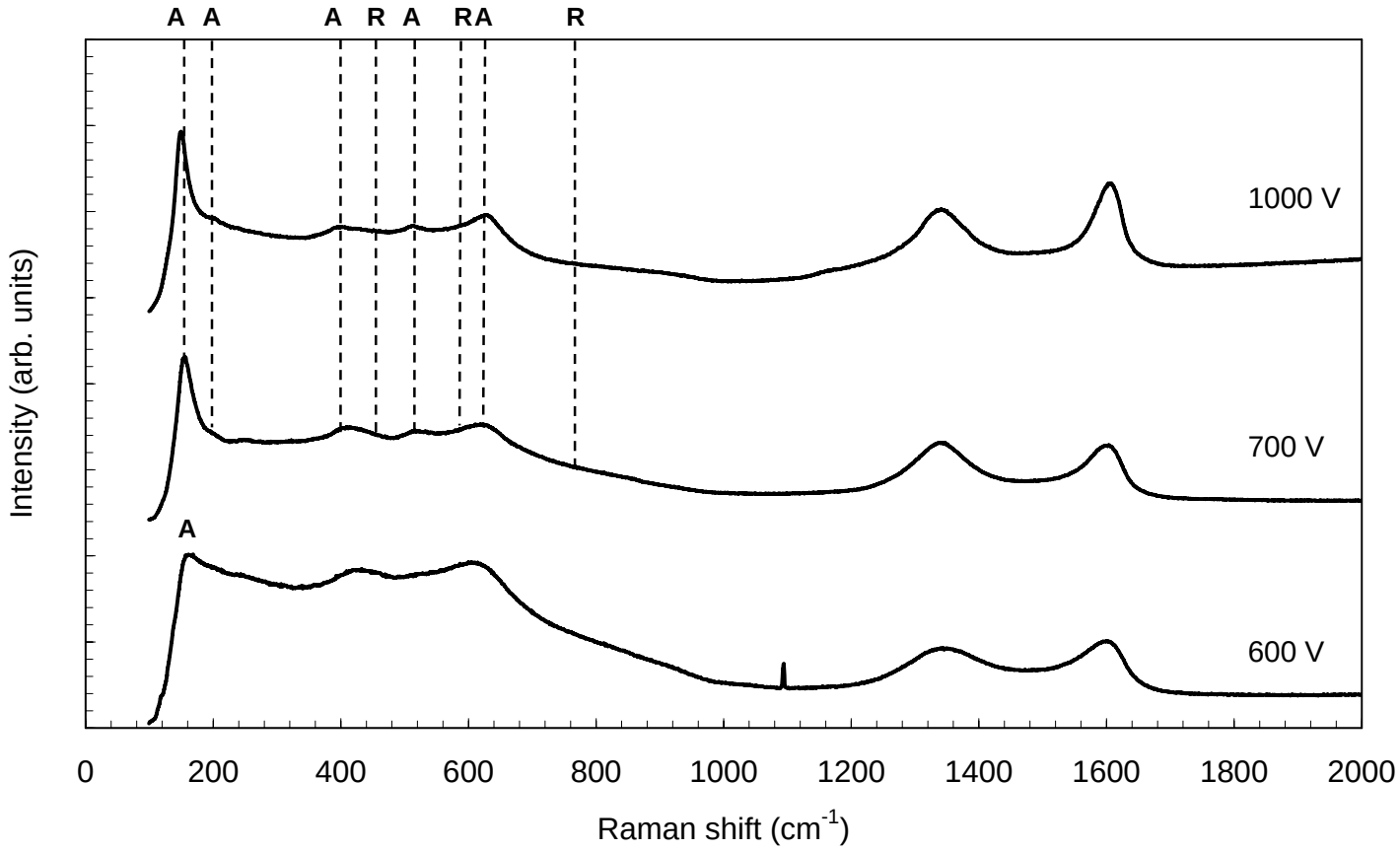
A A A R A RA R
1000 V
700 V
A
600 V
Intensity (arb. units)
0 200 400 600 800 1000 1200 1400 1600 1800 2000
Raman shift (cm-1)

Figure 5

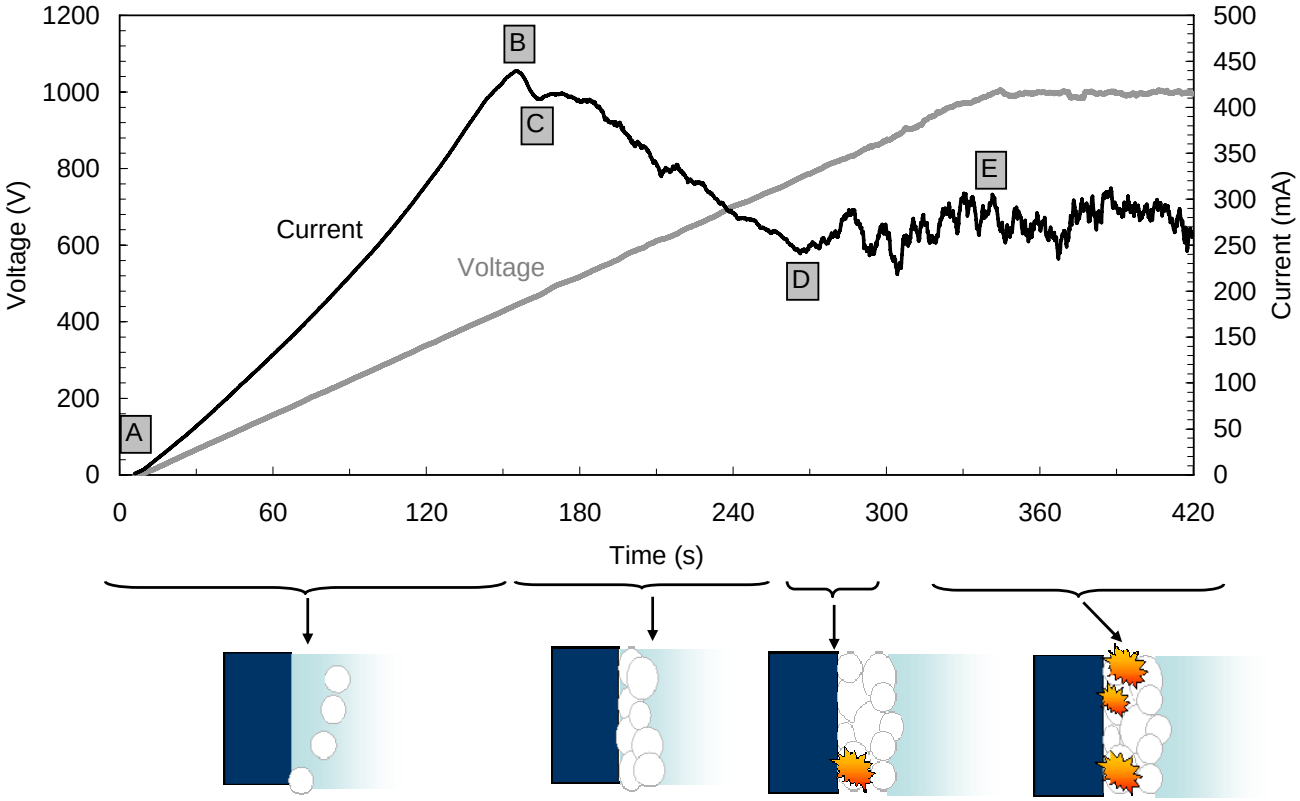
1200
1000
800
600
400
200
0
Voltage (V)
500
450
400
350
300
250
200
150
100
50
0
Current (mA)
0
60
120
180
240
300
360
420
Time (s)
A
B
C
D
E
Current
Voltage

Figure 6

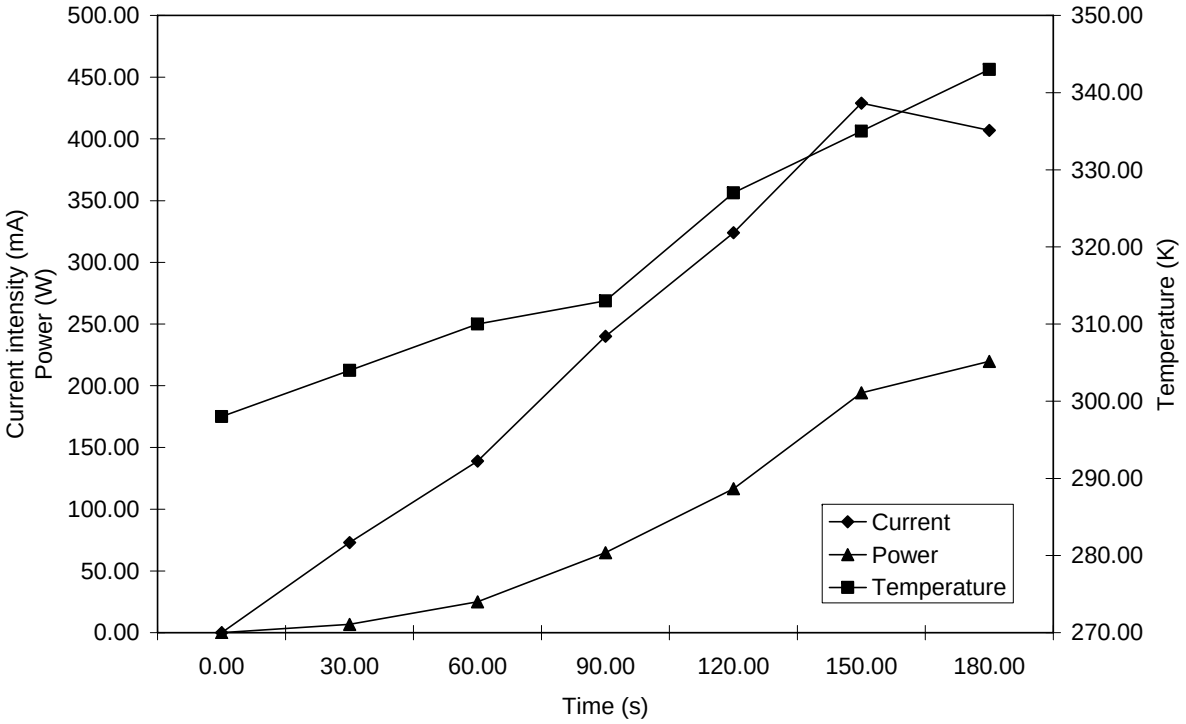
500.00
450.00
400.00
350.00
300.00
250.00
200.00
150.00
100.00
50.00
0.00
Current intensity (mA)
Power (W)
350.00
340.00
330.00
320.00
310.00
300.00
290.00
280.00
270.00
Temperature (K)
0.00
30.00
60.00
90.00
120.00
150.00
180.00
Time (s)
Current
Power
Temperature

Figure 7

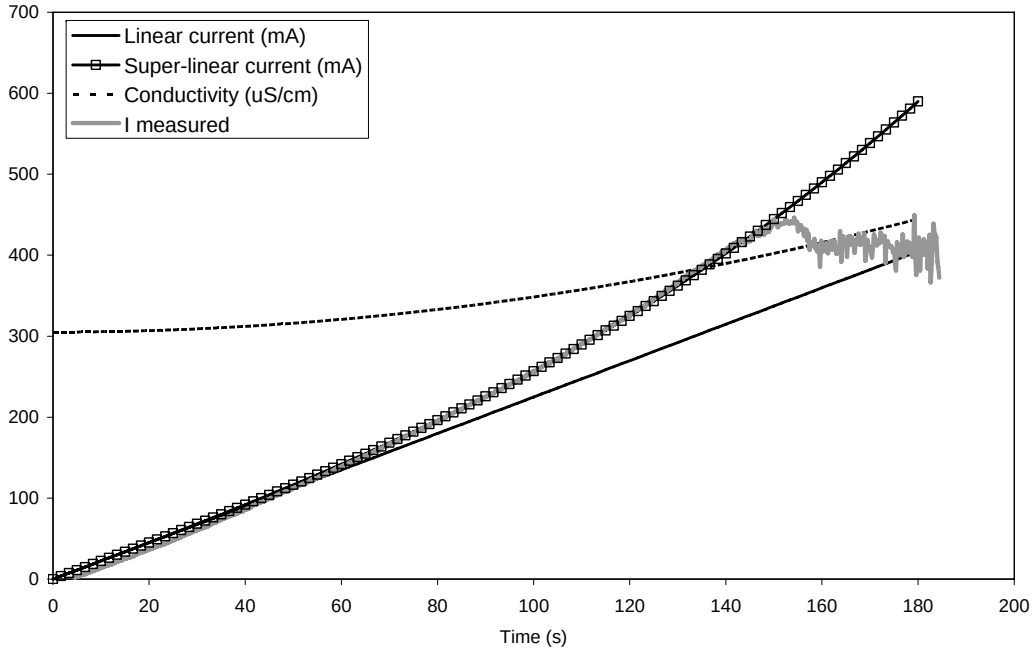
Linear current (mA)
Super-linear current (mA)
Conductivity (uS/cm)
I measured
700
600
500
400
300
200
100
0
0
20
40
60
80
100
120
140
160
180
200
Time (s)

Figure 8

	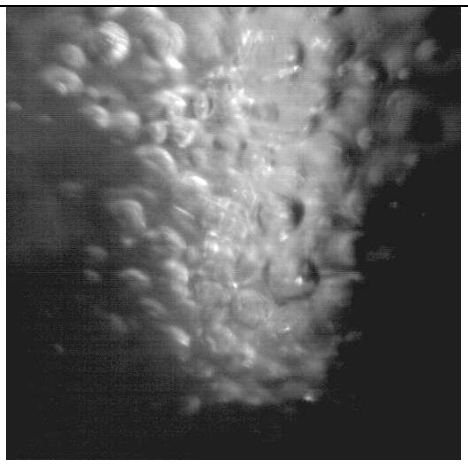	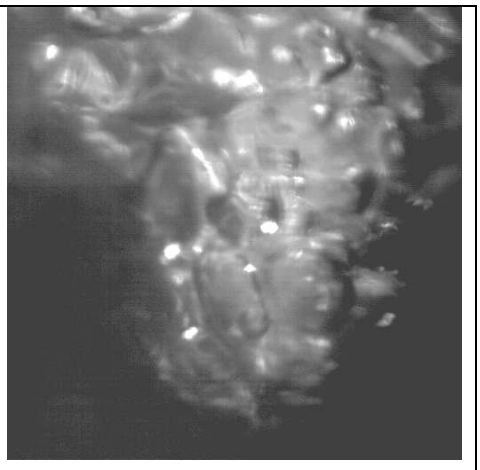
Voltage (V)	470	500
Current (mA)	412	372
Bubble radius (mm)	1	2
	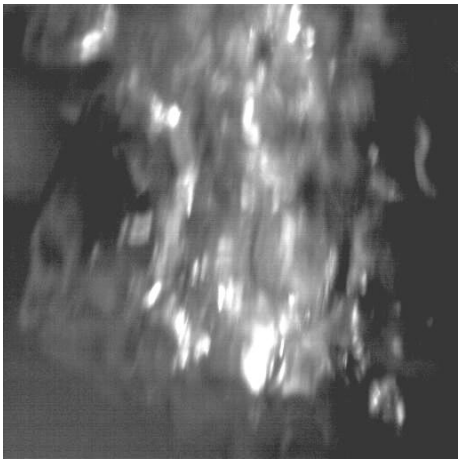	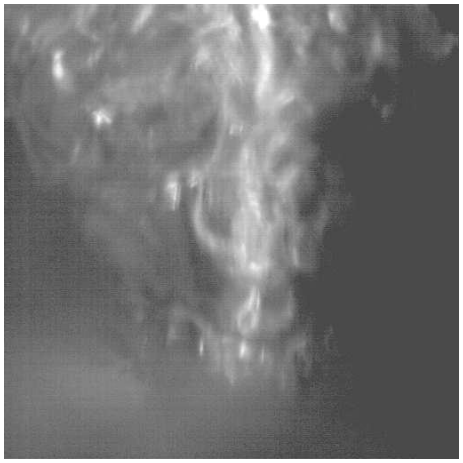
Voltage (V)	600	700
Current (mA)	350	290
Bubble radius (mm)	3	5

Figure 9

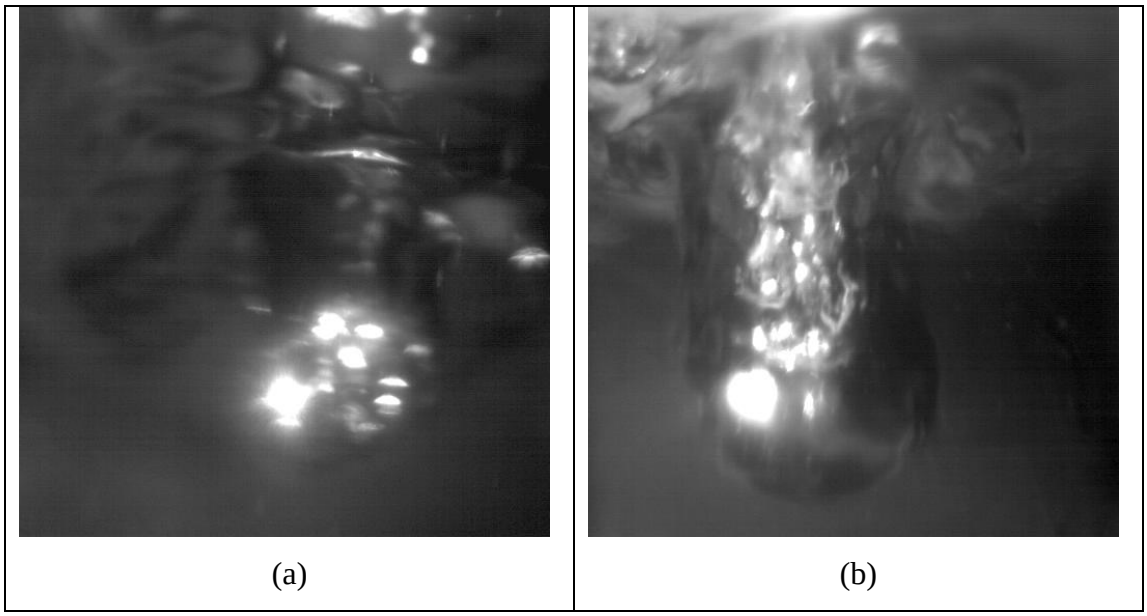

Figure 10

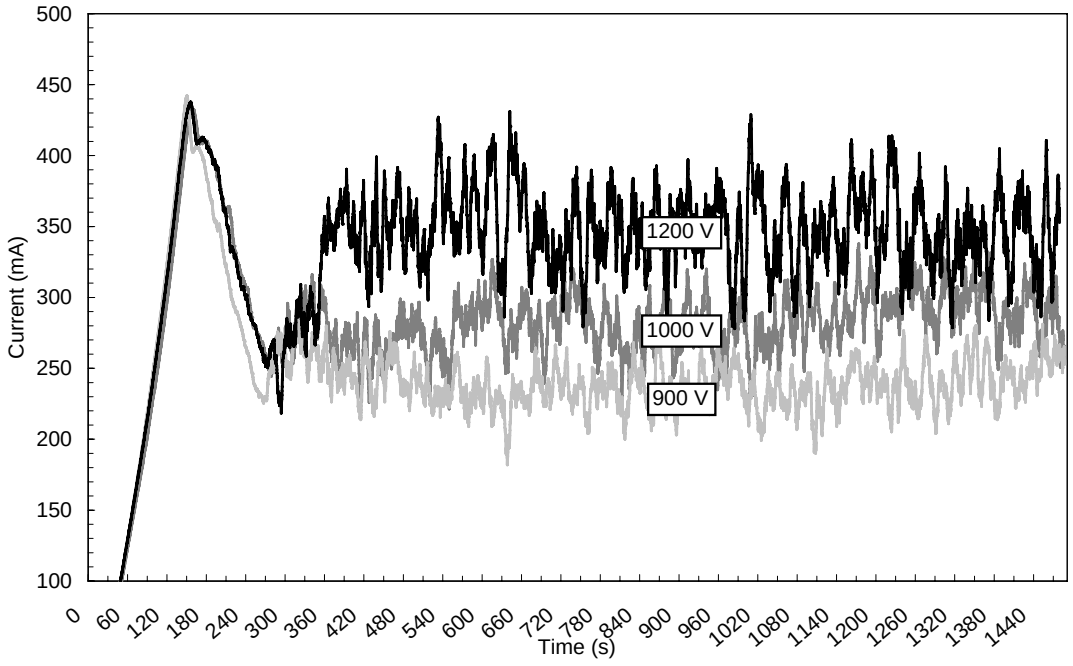

Figure 11

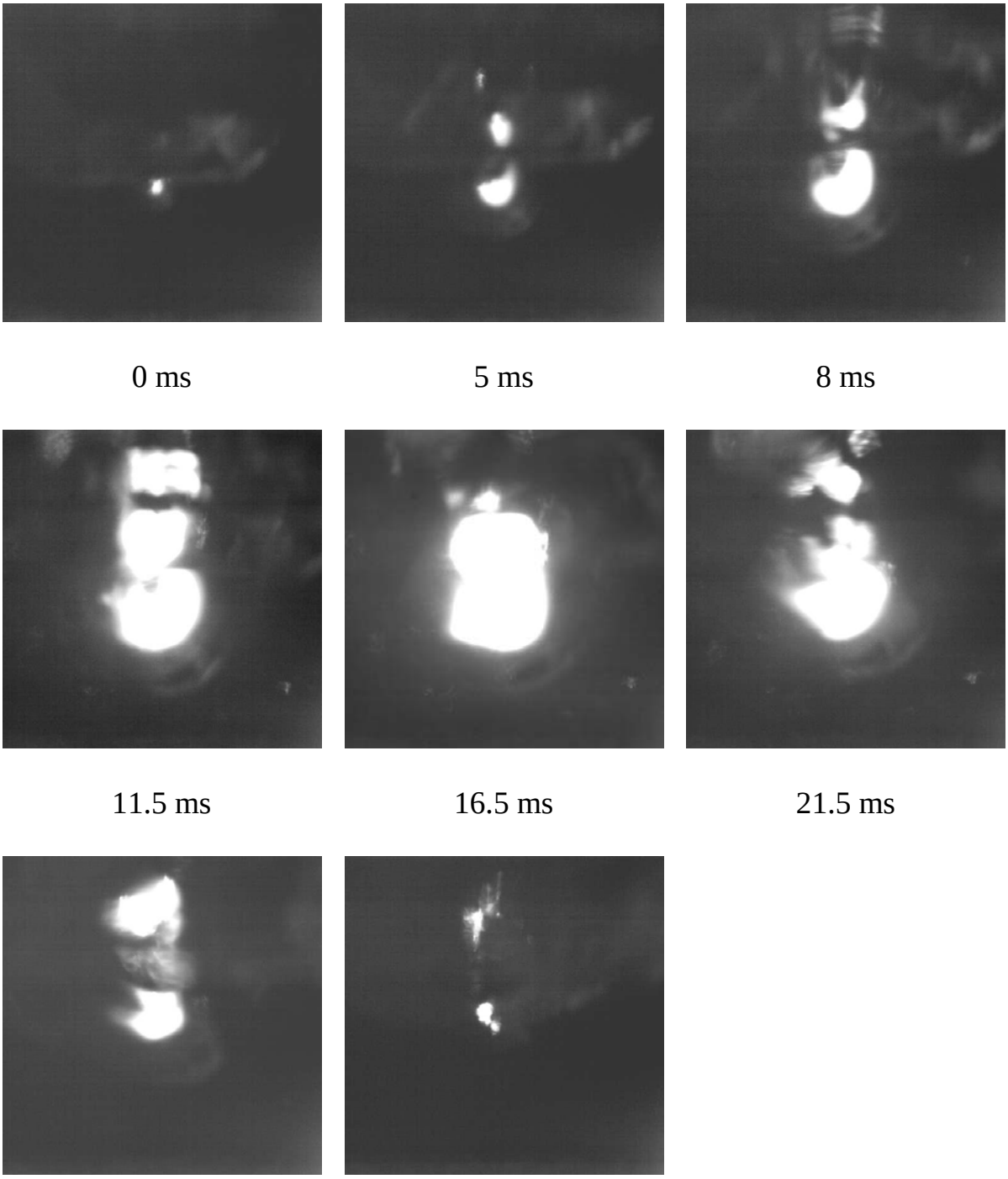

Figure 12

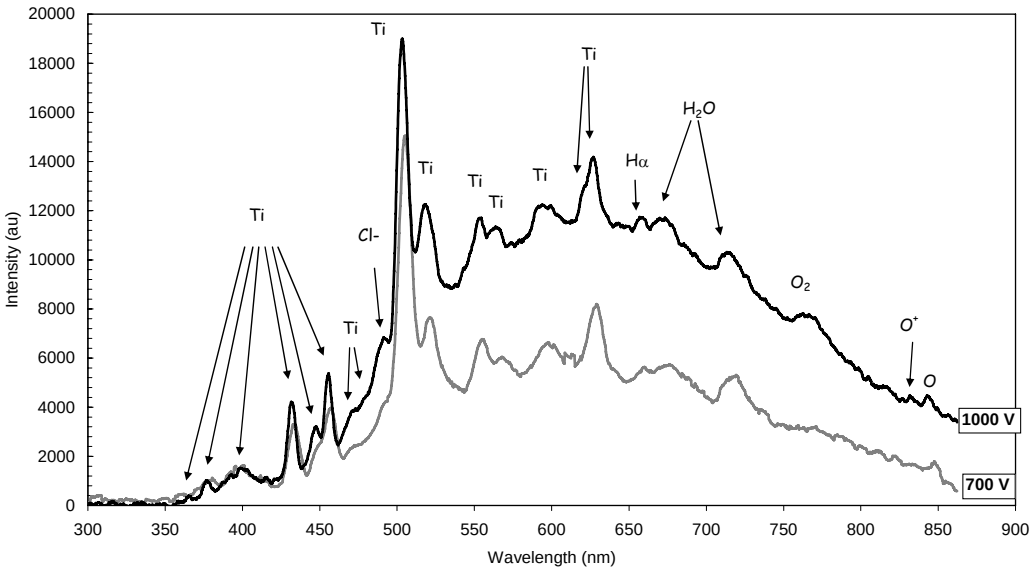

Figure 13

TABLES

Table 1

Applied voltage (V)	Mean discharge current (mA)	Mean discharge voltage (V)	Mean discharge power (W)
900	268	793	212
1000	300	880	264
1200	350	1060	371

Table 2

Line	λ (nm)	Transition	E (eV)	g	A (10^8 s^{-1})
1	501	5F-5G*	3.31	11	$6.43.10^{-2}$
2	517	3F-3F*	2.39	5	$3.8.10^{-2}$
3	625.8	3F-3G*	3.42	9	$8.36.10^{-2}$